J. Condensed Matter Nucl. Sci. 15 (2015) 81–91

Research Article

Imaging of an Active NANOR®-type LANR Component using CR-39*

Mitchell R. Swartz†, Gayle Verner, Jeffrey Tolleson, Leslie Wright, Richard Goldbaum
JET Energy Inc., Wellesley Hills, MA 02481, USA

Pamela Mosier-Boss and Peter L. Hagelstein
Research Laboratory of Electronics, Massachusetts Institute of Technology, Cambridge, MA 02139, USA

Abstract

This effort examined CR-39 chips exposed to a ZrO_2-PdD NANOR®-type CF/LANR component exhibiting significant energy. There was a fall-off in pit count with increasing distance from the operating system. Most interestingly, the CR-39 over the device essentially imaged the active CF/LANR device at very low resolution. Large tracks were the most effective for imaging. Smaller and mid-sized tracks appear to be useful for measuring fall off of the chip irradiation as a function of distance. The conclusion is that CF/LANR is a nuclear process, and for this system at this power level, the quantitative amount is measurable in a spatial, controllable, pattern.
 ISSN 2227-3123

Keywords: CR-39 Imaging, Imaging CF/LANR Systems, Preloaded CF/LANR component, ZrO_2PdD

1. Introduction

1.1. CF/LANR high energy emissions

Lattice assisted nuclear reactions (LANR) enable deuterium fusion under difficult-to-achieve conditions in hydrided Group VIII metals. Although LANR is a nuclear process, gamma emission is actually isospin forbidden by electric dipole transitions (both in charge independent [1] and dependent [2] analyses of the nuclear force). However, for hot fusion, the forbidden restriction is "lifted" by the high temperature, and so penetrating gamma emission is significantly observed. However at lower temperature, only rarely have charged particles, gamma radiation, and neutrons also been detected [3]. Past diligent efforts with autoradiography and CR-39 have heralded the recording of rare, high energy penetrating radiation emitted from cold fusion (LANR) materials in their active state; confirmed by autoradiography

*Confirmation of CF/LANR nuclear activity by emission of low level penetrating ionizing radiation which is temporally and spatially linked.
†E-mail: mica@theworld.com

 ISSN 2227-3123

or CR-39 chips over periods of days. Miles (China Lake, USN) and M. Srinivasan (Bhabha Atomic Research Center (BARC) independently used dental X-ray film autoradiography on the outside of the cells which revealed fogging heralding low energy X-ray production [4,5]. Srinivasan reported neutrons in 1989 as the current increased beyond 100 A, neutron signals, in bursts, resulted in 6 of 11 cells. Thereafter, energetic charged particles were detected by CR-39 in gas LANR systems [6] and in aqueous codeposition systems [7]. X. Z. Li (Tsinghua U) first used CR-39 in his 1990 Pd gas loading experiments to detect energetic charged particles [8].

Mosier-Boss et al. [7] reported CR-39 tracks which indicate possible neutron interactions, including carbon shattering. Some tracks herald D–D and DT reactions. Etching suggests uniformity in the 2–8 MeV range. The triple tracks, found in ∼5–10% of their experiments, indicate energetic neutrons have shattered carbon atoms. Also observed in LANR systems are mini-explosions, ionizing radiation, and neutron production, and tritium production. These observations of significant quantities of high energy charged particles, and emissions, in LANR systems, suggests that, although very few investigators have looked with adequate equipment, there is accumulating, near overwhelming, evidence that nuclear reactions in, and assisted by a lattice, are initiated at low energies. This paper describes how to image these systems (Fig. 1).

2. Experimental

2.1. Survey of problems

The first problem with quantitation by a detector is that only very low numbers of neutrons and charged particles with short range are emitted. The second problem is that if the emissions are similar to the near infrared (NT-NIR) emission (see Section 4.1) from active LANR materials, then such penetrating high energy emission should only occur when the CF/LANR devices are active at their optimal operating point (OOP). Third, the output from CF/LANR devices are

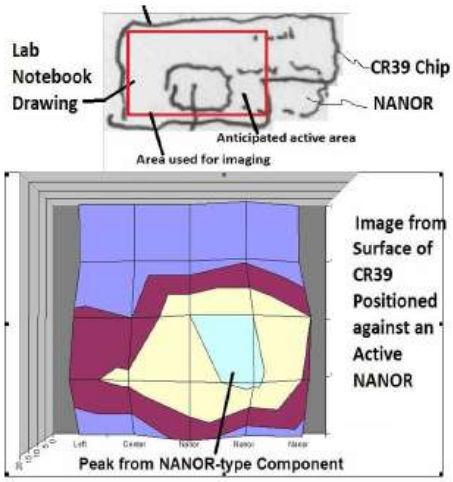

Figure 1. (a) (*left, top*) The location of the CR-39 chip over the NANOR®-type CF/LANR quantum electronic component. The ohmic control was at the top. (b) (left, *bottom*) This shows the distribution looking down the vertical axis, similar to the drawing above it. The very low resolution image of the NANOR® was obtained by pixel counting in the 2D record of large tracks on the CR-39 chip which was left vicinal to the NANOR®-type CF/LANR component. Another view is in Fig. 6b. There was no image from the ohmic control which was physically located just above the CF/LANR component, or in either of the two control CR-39 chips.

very low level and can be interfered with by environmental contamination (including people with ^{40}K). Therefore, a pretested NANOR®-type system was used at a number of input powers [8], run autonomously over days examined by Geiger Muller tube and CR-39, a polyallydiglycol carbonate polymer used as a time-integrating, solid state, nuclear track detector.

2.2. Materials

Nanostructured materials are important, unique and relevant to LANR and the future of LANR devices. They are used both as CF/LANR materials and produced in codeposition structures [9,3]. They have been observed producing non-thermal near infrared emissions when active [10], and exhibiting LANR excess heat correlated with the size of the Pd–D nanostructures [9]. Nanostructured materials have been used in LANR using palladium black [11] in a double structure (DS)-cathode. Today, second and third generation nanostructured ZrO_2–PdD and ZrO_2–PdNiD powders, such as Zr 67% Ni 29% Pd 4% (by weight before the oxidation step), absorb a very large number of deuterons for each and every nickel and palladium nuclei; with loading circa 3.5, and perhaps higher. LANR (CF) preloaded nanocomposite ZrO_2–PdNiD NANOR®-type CF/LANR components are capable of significant energy gain [12,14]. The ZrO_2–(Pd Ni)D is prepared with complicated processes of oxidizing and adding deuterons to the complicated mixture of zirconium oxide surrounding metallic palladium, nickel, or Pd-Ni islands. The air bake temperature and time, and final proprietary dopants and processing appear to have critical importance.

2.3. Methods – NANOR-type LANR device fabrication

We previously reported on the design and utilization of a new generation of active LANR (CF) preloaded nanocomposite ZrO_2–PdD and ZrO_2–PdNiD CF/LANR materials to fabricate NANOR®-type devices (Fig. 2) capable of significant, reproducible excess heat from applied electric fields [9,12,13]. These self-contained, two-terminal NANOR®-type LANR devices feature new composition, structure, and superior handling properties enabling portability and transportability. The NANOR®-type of LANR device used here contained active ZrO_2/PdD nanostructured material loaded with additional D. The deuterons are tightly packed ("highly loaded"). The additional D yields apparent indicated loadings (ratio to Pd) of more than 130% D/Pd, but shallow traps are not ruled out. For simplicity, all of these nanostructured materials in the core, in their range of deuterations, will henceforth simply be referred to as ZrO_2–PdD.

It is a long, expensive, arduous, effort to prepare these preloaded nanocomposite dry CF/LANR devices, whose development has required control of their breakdown states and quenching tendencies. The NANOR used for this work is a sixth generation CF/LANR device, smaller than 2 cm length, with less than a 50 mg of very active LANR material.

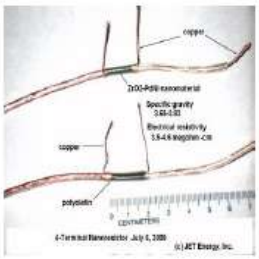

Figure 2. The source of the CF/LANR radiation which was imaged here, and detected by the irradiated CR-39 chip, is shown here. Two of these two terminal NANOR®-type devices containing active ZrO_2–PdNiD nanostructured material at their core are shown.

Although small in size, this is actually not *de minimus* because the LANR excess power density was more than 19,500 W/kg of nanostructured material [12]. The NANOR® system was driven for more than a year with careful evaluation for energy gain under a variety of conditions, including during the January, 2012 IAP MIT Course on CF/LANR, and later during a long term low-power open demonstration at MIT which ran from Jan. 30, 2012 through mid-May 2012 [12,13]. The NANOR®-type preloaded LANR device openly demonstrated clear cut energy gain and features including its convenient size and its superior handling properties. Over weeks, the NANOR®-type LANR device demonstrated reproducible, controllable, energy gain (COP) which ranged generally from 5 to 16 (e.g. 14.1 ($\sim$1412%) while the MIT IAP course was ongoing [13]).

2.4. Methods – electronic properties of nanomaterials

Close up, in ZrO_2–PdD LANR/CF nanostructured materials, the lattice of Pd is expanded by Zr, and less so, by the H and D. In addition, there are other major changes secondary to the oxidation of the Zr. Some are electrical and very important. The nanostructured material is a composite distribution of nanostructured ferromagnetic "islands" separated among a vast dielectric zirconia "ocean". The dielectric zirconia embeds uncountable numbers of nanostructured metal ternary alloy islands of the material containing now PdD. Electrically, the response of the CF/LANR nanostructured material is complex and characterized by complicated polarization/transconduction phenomena including an "avalanche effect" (transconduction electrical breakdown) which has a critical role in excess heat generation [9,12]. This occurs because the zirconia dielectric matrix is insulating at low voltage and it keeps the nanoscale metal islands electrically separated. We previously reported sudden changes of, and generally large, electrical impedances of such NANOR®-type devices containing nanostructured materials [9,12]. Several were $\sim$3 MΩ when lower voltages were applied, but then as the voltage was increased to $\sim$24 V, the impedance suddenly decreased to very low values. It was shown theoretically that this sudden reduction can be attributed to an "avalanche effect" that is typical of the current–voltage behavior that occurs in Zener diodes. Control and avoidance of low-threshold breakdown of states, the quenching tendencies of nanostructured materials, surmounting their extremely high electrical resistances and their complicated polarization/transconduction phenomena including said "avalanche effect" has a critical role in excess heat. Great difficulties had to be surmounted including assembly of apomaterials of very high electrical resistivity (impedance), as high as 300 GΩ, creating several serious problems. Therefore, a proprietary controlling system was used. This was designed with a complementary, surrounding calorimeter and a unique driving system whose design, autonomy, and interconnection implementations in conjunction with the NANOR®, have made portability of the system to MIT, and elsewhere, possible. The proprietary microprocessor controlled system semiquantitatively examines and drives the NANOR, examining it for heat-production activity, linearity, time-invariance, and even the impact of additives and applied fields.

The LANR preloaded, stabilized NANOR®s were driven by a high DC voltage circuit up to 1000^{+} volts rail voltage. The duty cycle was split with half going to a control portion consisting of a carefully controlled electrical DC pulse into an ohmic resistor which was used to thermally calibrate the calorimeter [12].

2.5. Methods – Data acquisition

Data acquisition (DAQ) was taken from voltage, current, temperatures at multiple sites of the solution, and outside of the cell, and even as a 4-terminal measurement of the NANOR's internal electrical conductivity [12,14]. Data acquisition sampling is at data rates of 0.20–1 Hz, with 24+ bit resolution; voltage accuracy of $0.015^{\pm 0.005}$ V, temperature accuracy $<$0.6°C). All connections are isolated when possible, including where possible with Keithley electrometers, or their equivalent, for computer isolation. The noise power of the calorimeter is in the range of $\sim$1–30 mW. The noise power of the Keithley current sources is generally $\sim$10 nW.

2.6. Methods – power and energy considerations

Input power is defined as $V \times I$. There is no thermoneutral correction in denominator. Therefore, the observed power is a lower limit. The instantaneous power gain (power amplification factor (non-dimensional)) is defined as $P_{\text{out}}/P_{\text{in}}$. The energy is calibrated by at least one electrical joule control (ohmic resistor) used frequently, and with time integration for additional validation. The excess energy is defined as $(P_{\text{output}} - P_{\text{input}}) \times$ time.

2.7. Methods – calorimetry

The amount of output energy (and therefore, both power, and energy, gain) is determined from the heat released producing a temperature rise, which is then compared to the input energy. Observed signals are determined by parallel diagnostics including thermometry, focused heat flow measurement, and isoperibolic calorimetry, and then semiquantitively repeatedly calibrated by an ohmic (thermal) control located next to the NANOR® [12].

The output of the NANOR® is compared to the output of the precisely-driven ohmic control. The instantaneous power gain is kinematically determined by the ratio of the input power normalized temperature increase to the input electrical power (P_{in}), called by the symbol 'HE/P_{in}' referring to the increase of temperature (ΔT) divided by the input electrical power. Also, the output of the NANOR® ΔT is independently derived by kinematically evaluating the heat flow, using the ratio of the input power normalized heat flow to the input electrical power (P_{in}), called by the symbol 'HF/P_{in}' referring to the heat flow (HF) divided by the input electrical power. The third method is examination by calorimetry, calibrated by the thermal ohmic control and thermal waveform reconstruction, and confirmed by long-term time integration. These three methods of verification are pooled to derive very useful information, including the energy produced ("excess energy") and sample activity. The result is heat measurement of this preloaded NANOR®-type LANR three ways ending in calorimetry, input-power-normalized ΔT (dT/P_{in}), and input power normalized heat (HF/P_{in}) [10].

2.8. Methods – setup

The CR-39 chips in this study were adjacent to, and were exposed to, a NANOR®, driven as a CF/LANR device Figs. 1a and 3). There was no pre-exposure of the chips to either O_2 or CO. A sample of chips had been exposed, on one corner, to a known alpha source, to ascertain that those induced tracts look consistent with expectations, confirming sensitivity and response. The track etch rate, used later after exposure, was determined from the known energy alpha track diameters (here, ^{241}Am, at $\sim$5.4 MeV less 256 keV lost traversing the oxide protective layer (e.g. Fig. 4b)). The resultant track diameters were, at their maximum, ca. 5–10 μm.

The entire setup was driven autonomously for several days to minimize exogenous irradiation of the chips. During LANR exposure, three CR-39 chips were used at different distances, and one was placed directly over the NANOR® during the irradiation sequence over several days. One CR-39 was partially shielded by several millimeters of aluminum within the chamber.

2.9. Methods – difficulties of working with CR-39

Many of the problems which exist in CR-39 analysis are partially surmounted here. These include relative insensitivity (which requires irradiation over long times), difficulty in resolving precise moieties, the need for electronic equilibrium including buildup (rarely considered), the possible interference by oxygen radicals generated near electrodes and by recombinant materials, heterogeneity over the CR-39, as well as a distribution including data recorded at different depths, and other various types of induced damage to the irradiated CR-39.

Therefore, for this experiment, long irradiation times were used (several days), buildup was achieved in part by the NANOR®s cylindrical shell, electrical insulation was made from all electrodes, and the active LANR nanomaterial

was dry with the detectors positioned over the potential emitter. After sectioning the image of the processed plate, the heterogeneity was used to image the device. Because there is information at a variety of levels (i.e. important information lies deep in the irradiated CR-39 chip), a system was engineered to extract this which will be a subject of a future paper. This permitted examination of the irradiated chip below additional "noise" secondary to irregular surfaces and changes wrought by the etching and handling of the chip.

2.10. Activity of the NANOR during monitoring

The driven NANOR did show excess energy during the experiment [15]. An M-NANOR® was used to maximize the likelihood of seeing some type of emitted output.

2.11. Quantifying the irradiated CR-39 chip

After the experiment, etching was performed using 6.5 Mol NaOH at 65°C for 8 h by Dr. Mosier-Boss. The surface noise was minimized by standard etching protocol to remove ∼6–10 μm from the CR-39 surfaces. The etch time created a distribution of maximum track diameters of circa ∼5–10 μm.

Examination of the processed CR-39 chips was done by optically sectioning each chip into 24 sectors away from the edges to remove handling errors. Large circular characteristic deep tracks, and paired large tracks, were counted. Counts were done by conventional optical microscopy and with side imaging which separates out surface noise from deeper tracks, and with a proprietary system which separates out surface noise from deeper tracks. The goal was to glean the information which lies deep in the chip below what appears to be a significant amount of "noise" secondary to irregular surfaces.

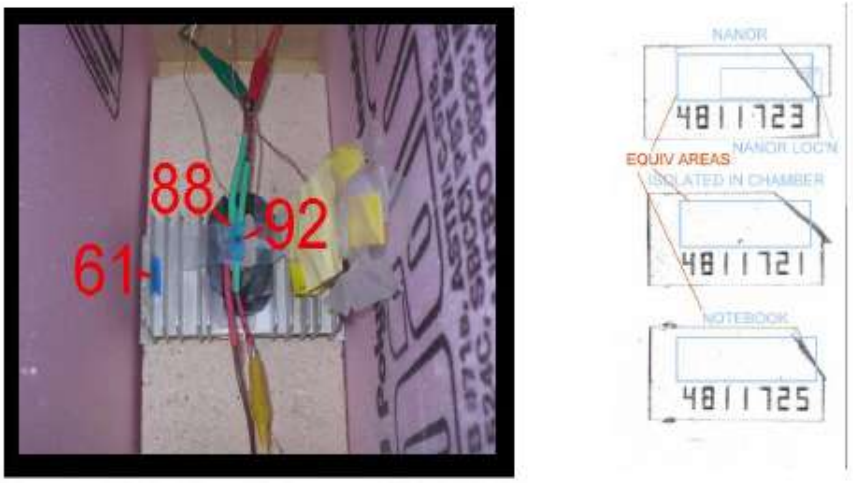

Figure 3. (a) (*left*) A look into the calorimeter which, for the photograph, has been stripped of thermal materials and probes to show the physical arrangement of the chips. For this image to show the location, all thermal ballast, addition thermal sensors, flow sensors, and addition insulation (both thermal and electrical) were removed. Shown are the NANOR® (beneath chip ′23, at the active site marked at #92, and the nearby chip, ′21, at site #61, which was partially shielded by aluminum. The NANOR is shown below the chip, with the darkened black region (site #92) believed to be the active area at the time. The CR-39 chip was placed above the NANOR, and then thermal materials and probes replaced before the experimental run. (b) (*right*) The three CR-39 chips with their ID numbers, hence forth ′23,′ 21, and ′25 (left in the lab notebook).

3. Results

3.1. Falloff with distance of irradiation of CR-39 chips

The collected, treated, examined chips did show incremental change, consistent with LANR activity, after they were scored (Figs. 4a and 5a,b). There was a fall-off in distance from the operating system (Figs. 5 and 6a).

3.2. Imaging of CCR-39 chips

For this system at this power level, the quantitative amount is measurable, and can give a spatial image (Figs. 1 and 6) if long periods of time are permitted in conjunction with control chips. This combination is used to remove the impact of exogenous sources of CR-39 irradiation, such as from environmental ^{40}K, environmental alphas, and spallation neutrons from irregularly irregular cosmic rays.

Large tracks were the most effective for imaging. Smaller and mid-sized tracks appear to be useful for measuring fall off of the chip irradiation as a function of distance.

3.3. Imaging of a CR-39 chip by an LANR component

Most interestingly, the CR-39 over the device had a final regional count post as shown in the figures below. Twenty-four pixels were used. Pixel by pixel, counts were made. In the figures below, the spatial homology is preserved except for rotation so that the back rows can be seen. It has essentially imaged the active CF/LANR device at very low resolution. The scalar count of the largest and paired tracks over the pixels, as we have done previously with positron

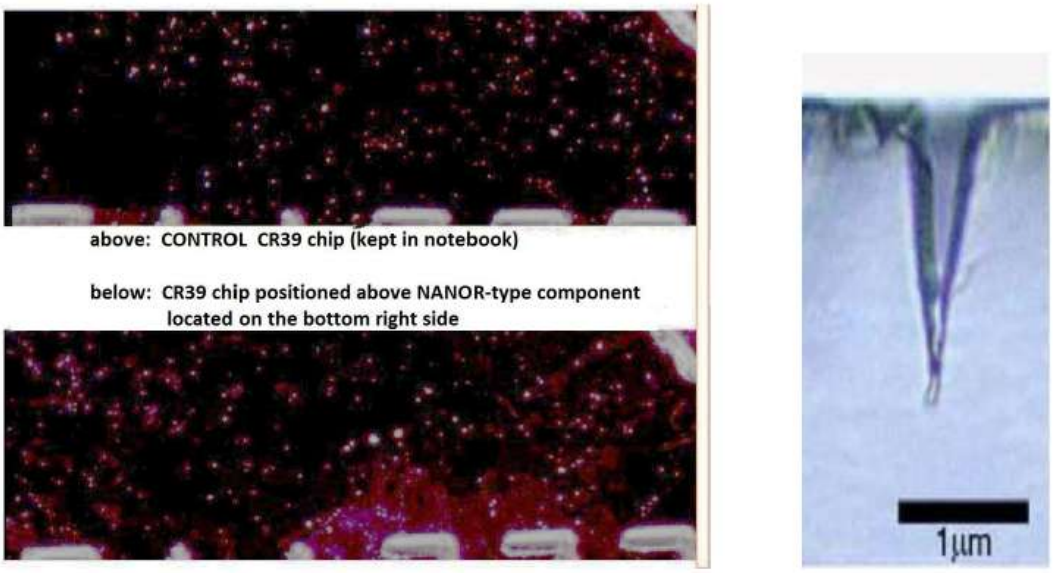

Figure 4. (a) (*left*) Actual images of two of the CR-39 chips (control kept in the notebook (*top*), and the one above the active NANOR (*bottom*). The NANOR was located on the bottom right. For this printing, there has been substantial image processing to brighten the image which would otherwise be too dark. The circles are the tracks seen in Fig. 4b in cross-section. (b) (*right*) Viewed from the side, an alpha track after etching on a CR-39 chip (after Yoshioka et al. [16]).

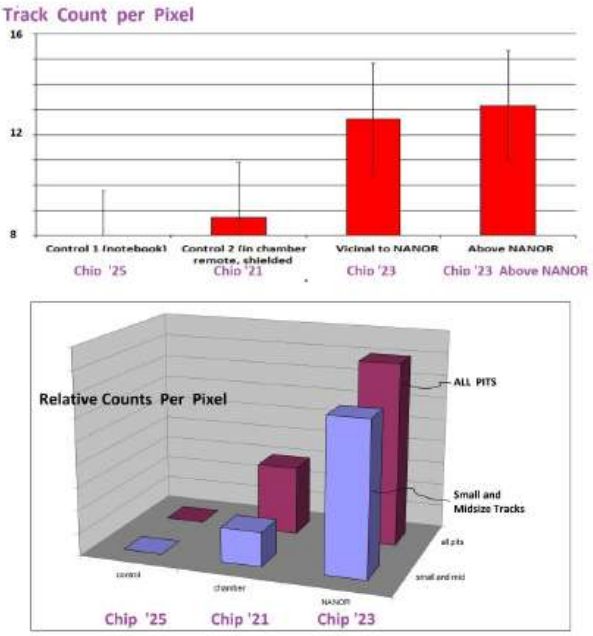

Figure 5. (a) (*top*) Histogram of small and medium sized circular defect densities (number per pixel) in the CR-39 chips which were located at a control location (notebook), in the chamber away from the NANOR®-type CF/LANR component and partially shielded by aluminum, and over the entire CR-39 chip covering the NANOR and nearby volume (defined 'vicinal'), as well as the area only directly above the NANOR. The error bars are 1 SD. (b) (*bottom*) Qualitative histogram of small and medium sized circular defects (blue) and all tracks (maroon) in the CR-39 chips. The counts are normalized to the control chip which was in the notebook .

emission tomography of tumors [17], reveals an "image" of the LANR/CF device elicited only after etching the CR-39 to derive the information "written" thereon.

4. Conclusions

4.1. Interpretation

LANR, as wrought by the NANOR®-type component, is a nuclear process. Furthermore, integrating emission-sensitive elements can, henceforth, be used to image the active site(s) of LANR systems, components, nanostructured materials and devices. It may also be useful for their study and development.

4.2. Questions to be answered

How much resolution can be obtained? How can it be offset with duty cycle? Can separate OOP manifolds now be measured for output and imaging? Do they occur at different locations in the NANOR or other CF/LANR component?

4.3. Possible etiology of the tracks in the CR-39

What is precisely the source of the tracks in the CR-39? Although it is relatively insensitive to gamma rays there could be additional contributions. A. Meulenberg has suggested that gammas energetic enough to create electron–positron

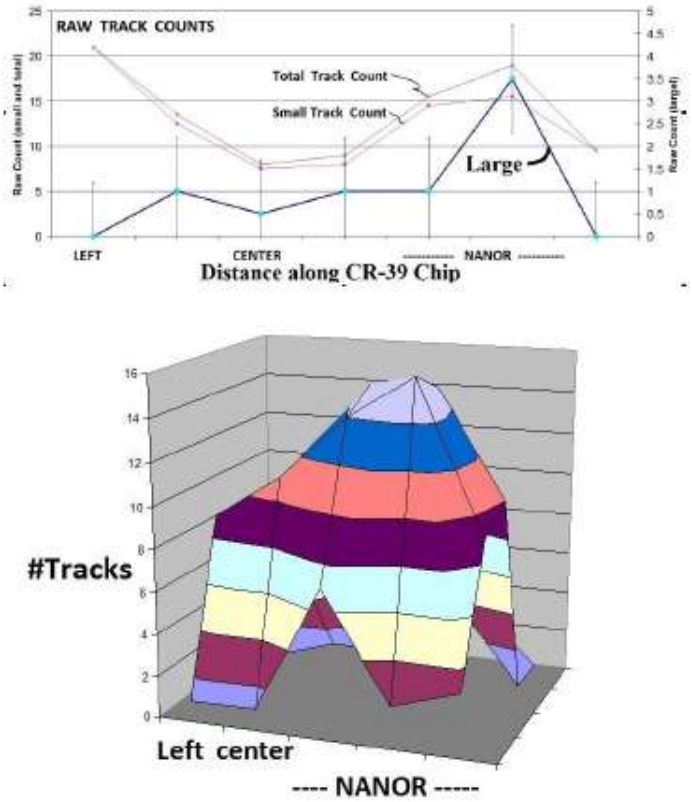

Figure 6. (a) (*top*) The distribution of the density of track counts of small tracks, all tracks, and large tracks as a function of location along a single chip place above the NANOR and the region around it. The NANOR was at the lower left of the flat chip. Importantly, it can be seen that large tracks may be the most useful in imaging CF/LANR systems. (b) (*bottom*) The distribution of density of the large tracks, pixel by pixel, is made over the surface of the CR-39 chip which covered the NANOR and its nearby region, as the NANOR ran continuously over days. Shown is a 3D representation of that large track density count, at this very low resolution pixel number, with the magnitude of the count shown by the height looking up the *y*-axis. With the same information, Fig. 1 shows the result of rotating this distribution and it shows how it looks directly down that *y*-axis. Also, confer Fig. 1b which shows the distribution from the vertical axis perpendicular to the long axis of the chip.

pairs might give a knock-on proton sufficient energy for a very short ionization path in the CR-39.

P. Mosier Boss and L. Forsley suggest an additional source might be triplet production [7]. In addition, a neutron can transfer half its energy to a proton, creating lengthy tracks. Furthermore, in rare conditions, tritium production has been seen [18,5]. However, tritum is unlikely etiology for three major reasons. First, because of the distance, second because of the very small amount which was ever producible, and third because the OOP manifolds are separate and the He-heat producing OOP manifold was mainly driven [19].

Could the results be due to IR or UV emission? Dr. Stan Szpak (SPAWAR) et al. reported the emission of infrared from LANR codeposition devices [20]. However, they did not use a control or calibration [10]. In 2008, Swartz demonstrated that two controls are needed, including normalization of NIR emission intensities to both non-energized background and to ohmic control areas.

In experiments involving a variety of LANR metamaterial spiral-wound and other Phusor®-type lattice assisted nuclear reaction (LANR) systems, including high impedance palladium [Pd/D_2O/Pt,Pd/D_2O/Au], codepositional (Pd/Pd$(OD)_2$/Pt) heavy water, and nickel (Ni/$H_2O_xD_2O_{1-x}$/Pt,Ni/$H_2O_xD_2O_{1-x}$/Au) light water Phusor®-type LANR devices. Swartz demonstrated that the emission of near-IR from the electrodes coupled with LANR operation is only observed when active electrodes operated at their optimal operating point, and that there was a linkage of excess power gain and heat flow with simultaneous NT-NIR emission [10].

Most importantly, NT-NIR is coupled and specific to the LANR devices' excess heat production and not its physical temperature. However, CR-39 is not effected by this low energy electromagnetic radiation unless sufficient to melt the material. Although that was not the case, high energy penetrating emission linked to CF/LANR excess heat, and transitions was the case, here.

Acknowledgements

The authors would like to thank Dr. Alex Frank, Alan Weinberg, Allen Swartz, Larry Forsley, Dr. Frank Gordon, Brian Ahern, Jeff Driscoll, Linda Hammond, Charles Entenmann, and Andrew Meulenberg for their suggestions. This effort was supported by JET Energy Inc. and New Energy Foundation. NANOR® and PHUSOR® are registered trademarks of JET Energy, Incorporated. NANOR®-technology, and PHUSOR®-technology are protected by U.S. Patents D596724, D413659 and several other patents pending.

References

[1] Radicati, L.A., *Phys. Rev*. **85** (1952) 962.
[2] Szydilik, P.P., Shell-model analysis of the excited states of ^{4}He, *Phys. Rev. C* **1** (1970) 1.
[3] Swartz, Mitchell M., Survey of the observed excess energy and emissions in lattice assisted nuclear reactions, *J. Scientific Exploration* **23**(4) (2009) 419–436.
[4] Miles, M. et al., Correlation of excess power and helium production during D_2O and H_2O electrolysis using palladium cathodes, *J. Electroanal. Chem.* **346** (1993) 99–117.
[5] Srinivasan, M. et al., Observation of tritium in gas/plasma loaded titanium samples. in anomalous nuclear effects in deuterium/solid systems, *AIP Conference Proceedings 228*, 1990. Brigham Young Univ., Provo, UT: American Institute of Physics, New York.
[6] Li, X.Z. et al., The precursor of cold fusion phenomenon in deuterium/solid systems, *AIP Conference Proceedings 228*, Brigham Young University, Provo, UT, New York, 1990.
[7] Mosier-Boss, P.A., Szpak, S., Gordon, F.E. and Forsley, L.P.G., Use of CR-39 in Pd/D co-deposition experiments, *Euro. Phys. J.–Appl. Phys.* **40** (2007) 293–303.
[8] Swartz, Mitchell R., Incremental emission from ZrO_2–Pd–D nanostructured CF/LANR quantum electronic component, *ICCF-18*, Missouri, USA, 2013.
[9] Swartz, Mitchell R., LANR nanostructures and metamaterials driven at their optimal operating point, *LANR/LENR Sourcebook*, Vol. 3, October 21, 2011.
[10] Swartz, Mitchell R., G. Verner and A. Weinberg, Non-thermal near-ir emission from high impedance and codeposition LANR devices, *Proc. ICCF-14*, Washington DC, USA, ISBN: 978-0-578-06694-3, 343, (2010).
[11] Arata, Y. and Y.C. Zhang, Observation of anomalous heat release and helium-4 production from highly deuterated palladium fine particles, *Jpn. J. Appl. Phys.* **38** (1999) L774–L776, Part 2, No. 7A, 1 July (1999).
[12] Swartz, Mitchell R., G. Verner and J. Tolleson, Energy gain from preloaded ZrO_2–PdNi–D nanostructured CF/LANR quantum electronic components, *ICCF17*, Daejeon, Korea, 2012.
[13] Swartz, Mitchell R. and P.L.Hagelstein, Demonstration of energy gain from a preloaded ZrO_2–PdD nanostructured CF/LANR quantum electronic device at MIT, *ICCF17*, Daejeon, Korea, 2012.
[14] Swartz, Mitchell R., Excess power gain using high impedance and codepositional LANR devices monitored by calorimetry, heat flow, and paired stirling engines, *Proc. ICCF-14*, Washington DC, USA, ISBN: 978-0-578-06694-3, 123, (2010)).

[15] Swartz, Mitchell R., P.L. Hagelstein et al., Amplification and restoration of energy gain using fractionated magnetic fields on ZrO_2–PdD nanostructured CF/LANR quantum electronic component, *ICCF-18*, Missouri, USA, 2013.
[16] I. Yoshioka, I Tsuruta, H. Iwano and I Danhara, *NucI. Instr. Method. Phys. Res. A* **555** (2005) 386.
[17] Kairento, A-E., G. Brownell, D. Elmaleh and Swartz, M.R., Comparative Measurement of Regional Blood Flow, oxygen and glucose utilisation in soft tissue tumour of rabbit with positron imaging, *Br. J. Radiology* **58** (1985) 637–643. .
[18] Iyengar, P.K. and M. Srinivasan, Overview of BARC studies in cold fusion, in *The First Annual Conference on Cold Fusion*, University of Utah Research Park, Salt Lake City, Utah: National Cold Fusion Institute, 1990.
[19] Swartz, Mitchell R., Optimal operating point manifolds in active, loaded palladium linked to three distinct physical regions, *Proc. ICCF-14*, Washington DC, USA, ISBN: 978-0-578-06694-3, 639, (2010).
[20] Swartz, Mitchell R., Codeposition of palladium and deuterium, *Fusion Technol.* **32** (1997) 126–130.